$[2_2](1,4)$cyclophane than in *anti*-$[2_2](1,3)$cyclophane, it is surprising that the two reductions of **7** and **8** show comparable potential separations (140 and 160 mV, respectively, Table Ib). Barring large structural rearrangements on complexation (an assumption supported by NMR evidence)[12,13] with a resulting change in $\pi-\pi$ interaction, the potential separation data indicate that the total Fe–Fe interaction is not composed solely of transannular interaction. Clearly, Fe–Ligand interaction contributes as well. Therefore if *anti*-$[2_2](1,3)$cyclophane complexes, with less transannular interaction, have a total interaction comparable to $[2_2](1,4)$cyclophane complexes, it must be due to a greater iron–ligand interaction in the *anti*-$[2_2](1,3)$-cyclophane complexes. This is consistent with the structure of the cyclophanes: *anti*-$[2_2](1,3)$cyclophanes, with a concave coordination site, are expected to have better overlap with metal orbitals than the $[2_2](1,4)$cyclophane with a convex coordination site.

If, as Langer and Lehner[38] concluded, there is no transannular interaction between the arene rings of *anti*-$[2_2](1,3)$cyclophane, one would expect a two-electron reduction for **8** corresponding to simultaneous reduction of both irons. The two one-electron reductions clearly indicate significant $\pi-\pi$ transannular interaction in *anti*-$[2_2](1,3)$cyclophanes, but this interaction cannot be quantitatively compared to that of other cyclophanes by measurement of potential separation without quantitative knowledge of the Fe–ligand interaction, solvation effects, and ion-pairing effects.

(37) Sato, T.; Torizuka, K.; Komaki, R.; Atobe, H. *J. Chem. Soc., Perkin Trans. 2* **1980**, 561.
(38) Langer, E.; Lehner, H. *Tetrahedron* **1973**, *29*, 375.

Conclusions

(1) CpFe(cyclophane) radicals are not as stable as other CpFe(arene) radicals, probably because the distortion of the arene ring affects the overlap of metal and orbital ligands.

(2) The redox potential dependence on cyclophane structure in the $CpFe^+$ series parallels the trend seen for HMB Ru^{2+} complexes. This suggests that redox potentials of the complexes depend upon the energy level of the π system in the ligand as well as on the extent of overlap of the metal and cyclophane orbitals.

(3) The complex of $[2_4](1,2,4,5)$cyclophane is the easiest to reduce and the most stable after reduction. The color and g values observed in the ESR spectrum of the radical suggest differences in the higher energy molecular orbitals, compared to other CpFe(arene) complexes.

(4) The degree of Fe–Fe interaction in $[(CpFe)_2(cyclophane)]^{2+}$ complexes, as measured by redox potential separation, depends on Fe–cyclophane interaction as well as $\pi-\pi$ transannular interaction within the cyclophane. The total Fe–Fe interaction is comparable for all bis(iron) complexes studied.

Acknowledgment. We thank A. Koray for a sample of **10** and E. D. Laganis, P. F. T. Schirch, and R. T. Swann for assistance in the preparation of **2**, **3**, and **4**. This work was supported at the University of Vermont by the National Science Foundation (Grants CHE80-04242 and CHE83-03974) and at the University of Oregon by National Science Foundation Grant CHE82-10282.

Registry No. **1**, 79105-26-3; **2**, 89890-15-3; **3**, 79554-76-0; **4**, 89890-17-5; **5**, 82429-41-2; **6**, 82433-58-7; **7**, 79169-87-2; **8**, 82433-63-4; **9**, 82433-65-6; **10**, 83679-01-0.

A Molecular Oribital Study of Bonding and Reactivity in Fe_4C Butterfly Clusters

Suzanne Harris* and John S. Bradley

Exxon Research and Engineering Company, Annandale, New Jersey 08801

Received January 18, 1984

We report the results of molecular orbital calculations for the Fe_4C butterfly clusters $[Fe_4C(CO)_{12}]^{2-}$, $[HFe_4C(CO)_{12}]^-$, $Fe_4C(CO)_{13}$, and $[Fe_4(CO)_{12}(C{\cdot}CO_2CH_3)]^-$. The structure of the clusters having an exposed carbon atom allows strong interactions between the carbido carbon and all four iron atoms in the cluster. In these clusters the molecular orbitals containing significant carbon character are stabilized, and the frontier orbitals are metal in character. The regioselectivity of the reactions interconverting $[Fe_4C(CO)_{12}]^{2-}$, $[HFe_4C(CO)_{12}]^-$, $HFe_4CH(CO)_{12}$, and $Fe_4C(CO)_{13}$ can be understood in terms of these metal frontier orbitals. The opening up of the iron butterfly that occurs when $Fe_4C(CO)_{13}$ reacts with methanol to form $[Fe_4(CO)_{12}(C{\cdot}CO_2CH_3)]^-$ weakens the interaction between the carbide carbon p orbitals and the wingtip iron atoms. This change in geometry, which makes the carbon p orbitals more accessible for bonding to a substituent, appears to be necessary for reaction to occur at the carbido carbon atom.

Introduction

One of the more intriguing recent results in cluster chemistry is the observation that the single carbon atom in carbido carbonyl clusters can be transformed from an inert structural unit in high nuclearity clusters (M_nC, $n \geq 5$) to a center of chemical reactivity when these larger clusters are partially fragmented to give M_4C clusters.[1,2] This phenomenon was first observed serendipitously in the reaction between $[Fe_6C(CO)_{16}]^{2-}$ and tropylium bromide in methanol giving the μ_4-methylidyne cluster $[Fe_4(CO)_{12}(C{\cdot}CO_2CH_3)]^-$ (eq 1).[3] Subsequent work in several laboratories has resulted in the establishment of a family of Fe_4C clusters.[4-6] The reactivity of the μ_4-carbon atom

(1) Tachikawa, M.; Muetterties, E. L. *Prog. Inorg. Chem.* **1981**, *28*, 203.
(2) Bradley, J. S. *Adv. Organomet. Chem.* **1983**, *22*, 1.
(3) Bradley, J. S.; Ansell, G. B.; Hill, E. W. *J. Am. Chem. Soc.* **1979**, *101*, 7417.

0276-7333/84/2303-1086$01.50/0

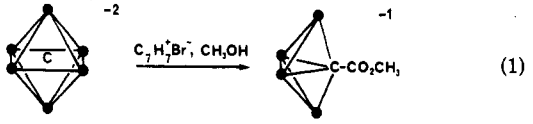

(1)

$[Fe_6C(CO)_{16}]^{2-}$ $[Fe_4(CO)_{12}(C{\cdot}CO_2CH_3)]^-$

in this class of compounds (in C–H and C–C bond-forming reactions) is of great interest not only intrinsically as organometallic cluster chemistry but also as a provacative model for the chemistry of carbon atoms adsorbed on metal surfaces.

In spite of the interest in these Fe_4C clusters, our understanding of both the bonding and reactivity of these clusters if far from complete. Kolis, Basolo, and Shriver examined several model Fe_nC clusters in an effort to understand the reactivity of the carbido carbon in the Fe_4C clusters,[7] while Housecroft and Fehlner considered the structure and bonding in $HFe_4CH(CO)_{12}$.[8] In order to gain a more general understanding of the unexpected reactivity of these molecules, we undertook a molecular orbital study of a series of Fe_4C clusters. Our aim was to relate the observed structures and reactivities of these clusters to their electronic structure. In this paper we first describe the results of Fenske–Hall molecular orbital calculations for $[Fe_4C(CO)_{12}]^{2-}$, $[HFe_4C(CO)_{12}]^-$, and $Fe_4C(CO)_{13}$ and use these results to form a basis for understanding the reactions interconverting these three molecules. Next we examine the reaction of $Fe_4C(CO)_{13}$ with methanol to give the μ_4-carbomethoxymethylidyne cluster $[Fe_4(CO)_{12}(C{\cdot}CO_2CH_3)]^-$.[4] Finally we describe the bonding in $[Fe_4(CO)_{12}(C{\cdot}CO_2CH_3)]^-$.[4] and contrast the structure and bonding in this C-derivitized cluster with that in the parent μ_4-carbide clusters.

Calculational Details

All of the results described in this paper were obtained from Fenske–Hall molecular orbital calculations.[9] The iron 1s through 3d basis functions were taken from Richardson et al.[10] while the 4s and 4p functions were chosen to have exponents of 2.0. The carbon and oxygen functions were taken from the double-ζ functions of Clementi.[11] The double-ζ 2p valence functions were retained while the 1s and 2s functions were reduced to single-ζ form. An exponent of 1.2 was used for hydrogen. Mulliken population analyses were used to determine atomic charges and orbital populations.

Calculations were carried out for several Fe_4C clusters whose crystal structures have been determined. The molecules $[Fe_4C(CO)_{12}]^{2-}$,[5] $[HFe_4(CO)_{12}]^-$,[12] $Fe_4C(CO)_{13}$,[4] and $[Fe_4(CO)_{12}(C{\cdot}CO_2CH_3)]^-$[3] are shown in Figure 1. Atomic positions in these clusters were idealized to C_{2v} (1a, 1b, 1c) and C_s (1d) symmetries from the known structures. Calculations were also carried out for several model clusters. The structures of these clusters are described in the text. In all the calculations described here the local coordinate system on the carbido carbon was oriented as shown in Figure 1 (i.e., the x axis parallel to a line connecting the two backbone irons, the y axis parallel to a line connecting the two wingtip irons, and the z axis pointing out of the cluster).

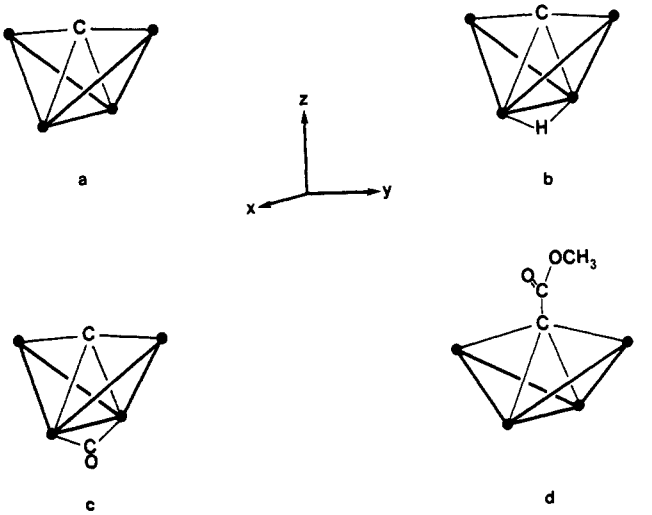

Figure 1. The structures of (a) $[Fe_4C(CO)_{12}]^{2-}$, (b) $[HFe_4C(CO)_{12}]^-$, (c) $Fe_4C(CO)_{13}$, and (d) $[Fe_4(CO)_{12}(C{\cdot}CO_2CH_3)]$. In all the clusters the carbido carbon atom lies in the mirror plane also containing the two backbone iron atoms. In d the organic group lies in this same plane. The local coordinate system on the carbon atom is defined so that the x axis is parallel to a line connecting the backbone iron atoms, the y axis is parallel to a line connecting the two wingtip iron atoms, and the z axis points out of the cluster.

1. Bonding in $[Fe_4C(CO)_{12}]^{2-}$. The simplest of the Fe_4C butterflies is $[Fe_4C(CO)_{12}]^{2-}$ (Figure 1a). For purposes of comparison we can envision the formation of $[Fe_4C(CO)_{12}]^{2-}$ from the fragments $[Fe_4(CO)_{12}]^{2+}$ and C^{4-}. This is of course hypothetical, but it alllows us to consider first the bonding in the iron butterfly fragment and to then consider the interaction of the iron butterfly with the carbon to form the iron butterfly carbide. The molecular orbital diagram for $[Fe_4(CO)_{12}]^{2+}$ is shown in Figure 2a. (The numbering of the orbitals in all of Figure 2 begins with the first orbital above the orbitals involving CO 5σ to Fe 3d donation in the $[Fe_4(CO)_{12}]^{2+}$ unit.) The distribution of levels in Figure 2a can be interpreted in terms of combinations of orbitals from the four $Fe(CO)_3$ fragments[13] making up the iron butterfly. The lowest 12 orbitals in the diagram, $1b_2$ through $2b_2$ and $3a_1$ through $3b_1$, are combinations of the filled "t_{2g}" orbitals from the $Fe(CO)_3$ groups. These orbitals are primarily nonbonding between the Fe atoms, so that their net contribution to any Fe–Fe bonding is negligible. Several of these orbitals do, however, have the proper orientation to interact with the missing carbon atom. The higher energy orbitals, beginning with $3a_2$, are combinations of the partially occupied frontier orbitals on the $Fe(CO)_3$ groups. These frontier orbitals derive from the octahedral e_g orbitals and a higher energy orbital containing iron 4s and 4p as well as 3d character. They are appropriately aligned for formation of Fe–Fe bonds in the Fe_4 butterfly cluster, so orbitals in $[Fe_4(CO)_{12}]^{2+}$ such as $3a_2$, $4b_2$, and $5a_1$ are bonding between the iron atoms. We will refer to these higher energy orbitals as the "e_g" set. In $[Fe_4(CO)_{12}]^{2+}$ the "e_g" levels are occupied only through $5a_1$ and as might be expected the $3a_2$, $4b_2$, and $5a_1$ orbitals are all metal–metal bonding. The four lowest energy-empty orbitals $4b_1$, $6a_1$, $5b_2$, and $7a_1$ also have considerable orbital character pointing in the direc-

(4) Bradley, J. S.; Ansell, G. B.; Leonowicz, M. E.; Hill, E. W. *J. Am. Chem. Soc.* **1981**, *103*, 4968.
(5) Davis, J. H.; Beno, M. A.; Williams, J. M.; Zimmie, J. A.; Tachikawa, M.; Muetterties, E. L. *Proc. Natl. Acad. Sci. U.S.A.* **1981**, *78*, 668.
(6) Whitmire, K. H.; Shriver, D. F. *J. Am. Chem. Soc.* **1981**, *103*, 6754.
(7) Kolis, J. W.; Basolo, F.; Shriver, D. F. *J. Am. Chem. Soc.* **1982**, *104*, 5626.
(8) Housecroft, C. E.; Fehlner, T. P. *Organometallics* **1983**, *2*, 690.
(9) Hall, M. B.; Fenske, R. F. *Inorg. Chem.* **1972**, *11*, 768.
(10) Richardson, J. W.; Nieupoort, W. C.; Powell, R. R.; Egell, W. F. *J. Chem. Phys.* **1962**, *36*, 1057.
(11) Clementi, E. *J. Chem. Phys.* **1964**, *40*, 1944; *IBM J. Res. Dev.* **1965**, *9*, 2.
(12) Holt, E. M.; Whitmire, K. H.; Shriver, D. F. *J. Organomet. Chem.* **1981**, *213*, 125.
(13) Elian, M.; Hoffmann, R. *Inorg. Chem.* **1975**, *14*, 1058.

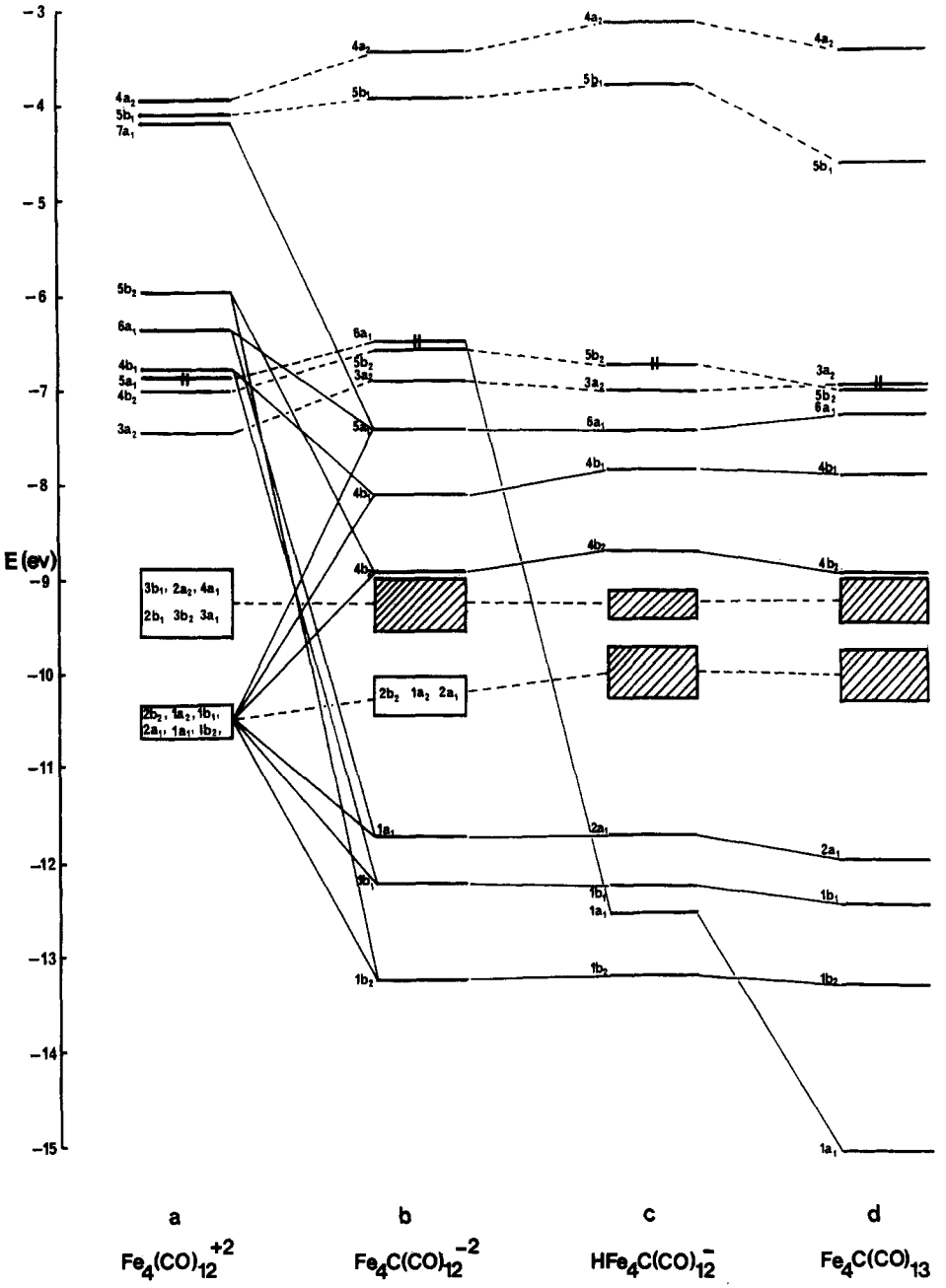

Figure 2. Molecular orbital diagrams for (a) $[Fe_4(CO)_{12}]^{2+}$ (in the same geometry as the dianion), (b) $[Fe_4C(CO)_{12}]^{2-}$, (c) $[HFe_4C(CO)_{12}]^{-}$, and (d) $Fe_4C(CO)_{13}$. The energy scale corresponds to the energies calculated for the levels in the neutral cluster $Fe_4C(CO)_{13}$. For purposes of comparison, the energies of the levels in the charged clusters have been scaled so that in each charged cluster the set of t_{2g} levels that does not participate in bonding with the carbido carbon orbitals lies at approximately the same energy as the corresponding set of levels in $Fe_4C(CO)_{13}$.

tion of the missing carbon atom and have the proper symmetry to accept electrons from the filled C^{4-} p_x, p_z, p_y, and p_z orbitals, respectively.

Figure 2b, the orbital diagram for $[Fe_4C(CO)_{12}]^{2-}$, reflects the interaction between the iron butterfly cluster orbitals and the carbon orbitals. A large number of the orbitals from the iron butterfly t_{2g} block do not interact with the carbon orbitals and therefore remain unaffected by the carbon's presence in the cluster. For purposes of comparison, this block of nonbonding orbitals in $[Fe_4C(CO)_{12}]^{2-}$ has been lined up approximately with the corresponding block in Figure 1a. The remaining orbitals will form the basis for discussion of the bonding in the dianion. The lowest energy orbitals $1b_2$, $1b_1$, and $1a_1$ have high carbon p_y, p_x, and p_z character, respectively. These orbitals are bonding between the carbon 2p orbitals and iron butterfly cluster orbitals from both the t_{2g} and e_g sets. Lying higher in energy, the $4b_2$, $4b_1$, and $5a_1$ orbitals are antibonding between the carbon p and iron cluster t_{2g} orbitals. They are thus pushed up in energy above the t_{2g} block of orbitals. The destabilizing effect of this antibonding interaction is counterbalanced somewhat, however, by the fact that these orbitals also contain a substantial bonding contribution from the $[Fe_4(CO)_{12}]^{2+}$ $5b_2$, $4b_1$, $6a_1$, and $7a_1$ "e_g" orbitals. Finally, the highest energy occupied orbitals are the Fe–Fe bonding orbitals $3a_2$, $5b_2$, and $6a_1$. These orbitals contain negligible carbon character.

Although all these orbitals are metal–metal bonding, the nature of the bonding in the three orbitals varies considerably. The $3a_2$ orbital 1 is bonding between the wingtip and backbone irons, with the bonds concentrated along the edges of the butterfly. The $5b_2$ orbital 2 is also bonding between the wingtip and backbone irons, but it is delocalized across the faces as well as the edges of the triangles

Table I. Overlap Populations

	$[Fe_4C(CO)_{12}]^{2-}$		$[Fe_4(CO)_{12}(C{\cdot}CO_2CH_3)]^-$	
	Fe_b[a]	Fe_w[b]	Fe_b	Fe_w
C (p_x)-Fe (d)	0.032	0.030	0.042	0.006
C (p_y)-Fe (d)	0.005	0.046	0.007	0.041
C (p_z)-Fe (d)	0.029	0.032	0.016	0.000
C (p_x)-Fe (d, s, p)	0.084	0.040	0.113	0.008
C (p_y)-Fe (d, s, p)	0.000	0.162	0.005	0.118
C (p_z)-Fe (d, s, p)	0.081	0.047	0.055	0.003
total C p-Fe (d, s, p)	0.165	0.249	0.173	0.129

[a] Backbone iron. [b] Wingtip iron.

formed by the backbone and wingtip irons. More important to the discussion to follow, this orbital also has lobes pointing away from the wingtip iron atoms and out of the cluster on the side of the carbido carbon. Finally, the HOMO, the $6a_1$ orbital **3** is bonding between the two backbone irons and is largely localized across these backbone iron atoms.

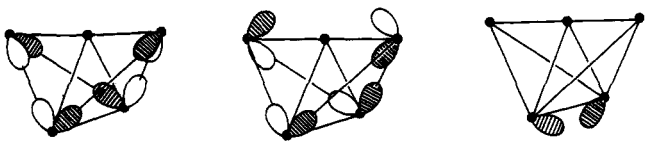

1 **2** **3**

The metal–carbon bonding can be described in the following way. The carbon p_z, p_x, and p_y orbitals interact with a_1, b_1, and b_2 orbitals, respectively, from both the t_{2g} and e_g sets of metal cluster orbitals. Since the levels containing both the bonding and antibonding interactions between the carbon and t_{2g} metal framework orbitals are occupied, the net contribution to metal–carbon bonding in the cluster from the interaction between these orbitals is negligible. On the other hand, the interaction between the carbon p and metal framework e_g orbitals produces a net bonding contribution since the antibonding orbitals are high in energy and only the bonding levels are occupied. The interactions that are important in this sense are shown schematically in **4**, **5**, and **6**. The carbon $2p_y$ orbital

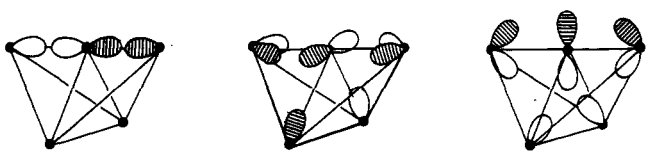

4 **5** **6**

interacts only with the wingtip irons, resulting in σ bonding between the carbon and wingtip iron atoms, **4**. The carbon $2p_x$ and $2p_z$ orbitals interact with both the backbone and wingtip irons. Interactions with the backbone are of a σ nature, while those with the wingtips are π in nature. The bonding combinations involving the carbon $2p_x$ and $2p_z$ orbitals are depicted in **5** and **6**, respectively.

The position of the carbon atom in this cluster, with the carbon and wingtip iron atoms being nearly colinear, tends to optimize the carbon σ bonding with both the wingtip and backbone Fe atoms and π bonding with the wingtip Fe atoms. The magnitudes of these σ and π interactions are reflected in the Fe–C overlap populations listed in Table I. It can be seen from Table I that the largest overlap population involving the iron d orbitals occurs between the carbon p_y and wingtip iron d orbitals. Although the overlap populations for the carbon p_x and p_z orbitals are smaller, the σ interactions with the backbone irons and the π interactions with the wingtip irons are comparable. These interactions, along with the interactions between the carbon p and iron 4s and 4p orbitals, result in the total C 2p–Fe overlap population being about 50% larger for the wingtip irons. Although overlap populations can only be an approximate measure of bond strength, the large difference in these values for the wingtip and backbone irons measures the importance of the interaction of the wingtip irons with all of the carbon 2p orbitals. This strong interaction between the carbon and wingtip iron atoms is reflected in the Fe–C distances in the cluster (1.78 Å for the wingtip iron vs. 1.95 Å for the backbone irons). Finally, a comment on the charge distribution in the cluster is in order, since a positive charge has been ascribed to the carbido carbon atom in order to explain both its large negative ^{13}C NMR chemical shift[14,15] and its apparent electrophilicity. In fact, our calculations show that the carbido carbon atom carries a net negative charge (approximately −0.6). Although the exact value of the calculated charge should be treated with some caution, the significant size of the calculated value indicates that the carbido carbon atom is not positively charged. The NMR data probably reflect paramagnetic contributions to the chemical shift (see comment by E. W. Randall[14]). The reactivity of the carbon atom, which was also claimed to reflect cationic character,[3,13] is discussed below.

In summary, the carbido carbon atom is bound to all four iron atoms, through σ interactions with the backbone carbons and both σ and π interactions with the wingtip irons. The nearly colinear arrangement of the carbido carbon and wingtip iron atoms makes it possible for all three of the carbon p orbitals to interact with the wingtip iron atoms. In contrast to the results of Shriver[7] for model Fe_4C clusters (in those calculations all the $Fe(CO)_3$ groups were replaced by FeH groups), we find that the three highest energy occupied orbitals are associated with metal framework bonding and have essentially *no carbon character*, whereas the occupied orbitals that do contain significant carbon character lie lower in energy than these metal framework orbitals. The HOMO–LUMO gap in this cluster is calculated to be large (approximately 2.5 eV), in accordance with Lauher's[16] predictions about the stability of the butterfly configuration for a 62-electron system. Once again in contrast to the results of Shriver we find that the LUMO and the next highest empty MO have no carbon character. Instead the first unoccupied orbital having carbon character lies approximately 4.4 eV above the HOMO. The fact that the frontier orbitals are predominantly metal in character is consistent with the observed reactivity of the cluster, and in the next section we consider the protonation of $[Fe_4(CO)_{12}]^{2-}$ to form $[HFe_4C(CO)_{12}]^-$ and the oxidation of $[Fe_4C(CO)_{12}]^{2-}$ in the presence of CO to form $Fe_4C(CO)_{13}$.

2. Bonding in $[HFe_4C(CO)_{12}]^-$ and $Fe_4C(CO)_{13}$. At first sight it might be expected that reaction with H^+ would result in protonation of the carbido carbon atom, since in $[Fe_4C(CO)_{12}]^{2-}$ the carbido atom carries a significant negative charge (this is true for all the Fe_4C clusters considered here). Instead, the proton adds across the backbone iron–iron bond to give $[HFe_4C(CO)_{12}]^-$ (Figure 1b). The site of protonation is consistent with the orbital structure of $[Fe_4C(CO)_{12}]^{2-}$, since in $[Fe_4C(CO)_{12}]^{2-}$ the HOMO and other high-energy occupied orbitals are metal framework bonding orbitals. Despite the negative charge on the carbon atom, protonation at this site is precluded by the fact that the high-energy occupied orbitals contain

(14) Bradley, J. B. *Philos. Trans. R. Soc. London, Ser. A* **1982**, *308*, 103.
(15) Albano, V. G.; Chini, P.; Martinengo, S.; McCaffrey, D. J. A.; Strumolo, D.; Heaton, B. J. *J. Am. Chem. Soc.* **1974**, *96*, 8106.
(16) Lauher, J. W. *J. Am. Chem. Soc.* **1978**, *100*, 5305.

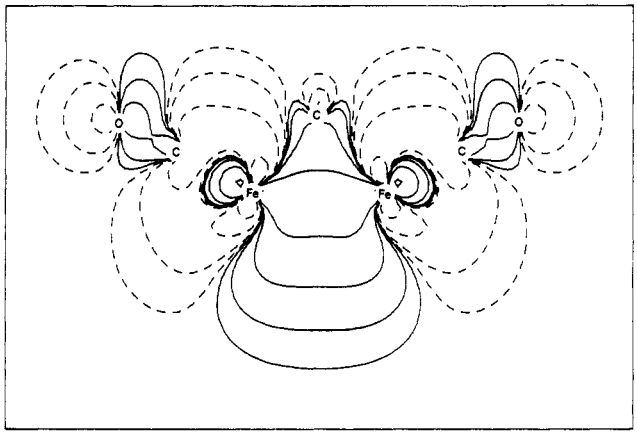

Figure 3. Orbital plot of the $6a_1$ orbital of $[Fe_4C(CO)_{12}]^{2-}$ in the plane containing the two backbone iron atoms and the carbido carbon atom.

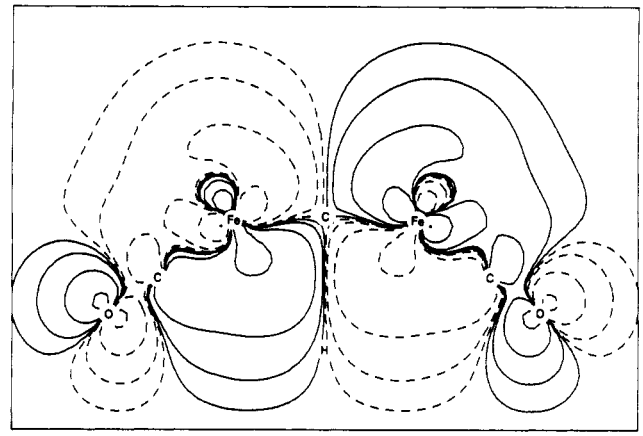

Figure 4. Orbital plot of the $5b_2$ orbital of $[HFe_4C(CO)_{12}]^-$ in the plane that contains the two wingtip iron atoms and the carbido carbon atom and bisects the backbone of the butterfly.

no carbon character. A contour plot of the $6a_1$ orbital (taken through the plane containing the carbido atom and the two backbone iron atoms) is shown in Figure 3, and it is this orbital, the HOMO, with which the proton interacts. The result of this interaction can be seen from the orbital diagram for $[HFe_4C(CO)_{12}]^-$ (Figure 2c). The only real difference between parts b and c of Figure 2 is the disappearance in Figure 2c and of the $6a_1$ orbital as the HOMO and the appearance of a new $1a_1$ orbital (the bonding combination of the hydrogen 1s and $[Fe_4C(CO)_{12}]^{2-}$ $6a_1$ orbitals) among the carbon–iron bonding orbitals. Examination of both the character of the orbitals and the overlap populations for $[HFe_4C(CO)_{12}]^-$ shows that except for a sharp decrease in the overlap populations between the two backbone iron atoms, the Fe_4C cluster remains essentially unchanged by the addition of H^+. It should be noted, however, that the $5b_2$ orbital now becomes the HOMO. As described above, this orbital is bonding between the backbone and wingtip iron atoms, **2**, but it also has directional properties that are important for the addition of a second proton to this cluster. It was shown by Tachikawa and Muetterties[17] that when a second proton adds to this cluster it bridges the carbido carbon and one of the wingtip iron atoms. The formation of this cluster is consistent with the orbital structure of $[HFe_4C(CO)_{12}]^-$. A contour plot of the HOMO, $5b_2$, of $[HFe_4C(CO)_{12}]^-$ (taken through the plane containing the carbido carbon and the two wingtip irons) is shown in Figure 4. The plot shows that this orbital has lobes pointing out of the cluster above the carbido carbon. Certainly, interaction of the proton with this orbital followed by a slight rearrangement of the cluster to allow bonding with the carbido carbon as well as the wingtip iron atom is reasonable. The bonding in $HFe_4CH(CO)_{12}$ has been described by Housecroft and Fehlner[8] and is consistent with this interpretation.

A third Fe_4C cluster that can be derived from $[Fe_4C(CO)_{12}]^{2-}$ and that has a similar structure is $Fe_4C(CO)_{13}$ (Figure 1c).[4] In this cluster, which can be formed by oxidation of $[Fe_4C(CO)_{12}]^{2-}$ in the presence of CO[5], the thirteenth CO bridges the two backbone iron atoms. This reaction can be understood by considering once again the orbital diagram for the dianion (Figure 2b). Oxidation of the dianion could remove two electrons from the HOMO $6a_1$ orbital. Our calculations confirm that in a hypothetical neutral $Fe_4C(CO)_{12}$ cluster having the same structure as the dianion, the LUMO becomes the $6a_1$ orbital. This orbital lies very close in energy above the occupied $5b_2$ orbital and is still localized across the backbone irons. It follows then that an attack on the oxidized cluster by the nucleophile CO would result in the addition of CO across the backbone. The orbital structure of $Fe_4C(CO)_{13}$ confirms that the $6a_1$ orbital of the dianion interacts with the CO molecule (Figure 2d). Just as for $[HFe_4C(CO)_{12}]^-$, the only significant difference between the diagram in Figure 2d and that for the dianion in Figure 2b is the disappearance of the $6a_1$ orbital as the HOMO and the appearance of a new lower energy $1a_1$ orbital. This new a_1 orbital results from the bonding interaction between the $6a_1$ cluster orbital and the bridging CO 5σ orbital. Once again, except for a decrease in the overlap populations between the backbone iron atoms, the structure and bonding of the Fe_4C cluster itself is not disrupted by the addition of the bridging CO.

The above discussion indicates that the reactivity of $[Fe_4C(CO)_{12}]^{2-}$ initially involves orbitals associated with the metal framework rather than the carbido carbon. The geometry of the cluster allows strong interactions between the carbido carbon orbitals and the iron butterfly framework orbitals. These interactions stabilize the carbon orbitals to such an extent that the reactivity of the cluster involves only the higher lying metal framework orbitals. As a result, the formation of $[HFe_4C(CO)_{12}]^-$ and $Fe_4C(CO)_{13}$ comes about by the interaction of the $6a_1$ cluster orbital with the incoming H^+ or CO. The attack of a second H^+ on the dianion appears to initially proceed via interaction with the $5b_2$ cluster orbital, also a metal framework orbital. The subsequent bond formation with the carbido carbon atom requires a rearrangement of the cluster. Therefore no reaction of $[Fe_4C(CO)_{12}]^{2-}$ appears to occur via a direct attack on the carbido carbon atom.

3. Carbon–Carbon Bond-Forming Reactions of $Fe_4C(CO)_{13}$. Although the first example of a C-derivitized Fe_4C cluster was found in the reaction of an Fe_6C precursor, the intermediacy of $Fe_4C(CO)_{13}$ in the complex reaction summarized by eq 1 has been established.[18] In fact, $Fe_4C(CO)_{13}$ undergoes a number of C–C bond-forming reactions.[14] One of the goals of this study was to understand this reactivity in terms of the structure and bonding in the cluster and to explain the change in the geometry of the Fe_4C unit that occurs when the carbon atom becomes part of an organic group (see below). The most thoroughly studied example of reactivity at the carbido carbon atom, giving a C-derivitized butterfly cluster, is provided by the reaction between $Fe_4C(CO)_{13}$ and meth-

(17) Tachikawa, M.; Muetterties, E. L. *J. Am. Chem. Soc.* **1980**, *102*, 4541.

(18) Bradley, J. S.; Hill, E. W.; Ansell, G. B.; Modrick, M. A. *Organometallics* **1982**, *1*, 1634.

anol.[4,14] This reaction yields $[Fe_4(CO)_{12}(C{\cdot}CO_2CH_3)]^-$ (Figure 1d), in which the butterfly arrangement of the iron atoms is maintained while the μ_4-carbido carbon atom is bound to the carbon atom of the $COOCH_3$ group. In this section we discuss a possible pathway for this reaction; in the following section we describe the bonding in the product $[Fe_4(CO)_{12}(C{\cdot}CO_2CH_3)]^-$. As we saw in the preceding sections, the structure of the clusters containing an exposed carbon atom, i.e., the nearly colinear arrangement of the carbido carbon and wingtip iron atoms, imparts stability to the carbon orbitals and thus precludes reactivity of the carbon atom itself. In $[Fe_4(CO)_{12}(C{\cdot}CO_2CH_3)]^-$, the wingtip iron atoms are folded back so that the distance between the wingtip irons and carbido carbon increases to 2.02 Å and the Fe–C–Fe angle for the wingtip irons decreases to 148°. (The corresponding distance and angle in $[Fe_4C(CO)_{13}]$ are 1.80 Å and 175°.) The folding back of the wingtip irons is also accompanied by a significant decrease in the average distance between the wingtip and backbone iron atoms (2.50 Å in $[Fe_4(CO)_{12}(C{\cdot}CO_2CH_3)]^-$ vs. 2.64 Å in $[Fe_4C(CO)_{13}^{2-}]$). The distances and angles involving the carbido carbon and backbone irons are not changed significantly. A major consequence of the change in structure, as we will see in our discussion of the bonding in $[Fe_4(CO)_{12}(C{\cdot}CO_2CH_3)]^-$, is a loss of the π interactions between the carbido carbon p_x and p_z and wingtip iron orbitals. This change in structure may also play an important role in the actual formation of $[Fe_4(CO)_{12}(C{\cdot}CO_2CH_3)]^-$ from $Fe_4C(CO)_{13}$.

The mechanism for the reaction between $Fe_4C(CO)_{13}$ and methanol has been the subject of considerable interest and speculation. One proposed pathway[14] for the reaction involves the formation of a ketenylidene intermediate that then reacts with CH_3OH to give the product ester (eq 2).

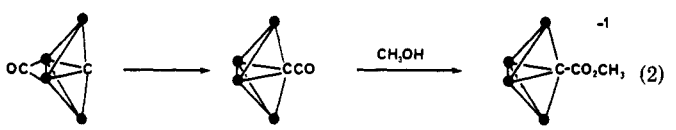

(2)

$Fe_4C(CO)_{13}$ $Fe_4(CO)_{12}(CCO)$ $[Fe_4(CO)_{12}(C{\cdot}CO_2CH_3)]^-$

Although it is well-known that the carbonyl ligands in metal carbonyl clusters readily migrate around the metal cluster framework, the formation of the ketenylidene from $Fe_4C(CO)_{13}$ requires the migration of a carbonyl ligand not just around the metal framework but onto the carbido carbon atom as well. The discussion in the last section suggests that migration onto the carbido carbon atom is unlikely, since the stabilized carbido carbon orbitals in the cluster would be unavailable to interact with the CO orbitals. Consequently, as long as the Fe_4C cluster geometry is maintained, we would not expect the carbonyl to migrate across the carbido carbon atom. The reaction we are considering here, however, results in a change in geometry of the Fe_4C framework, and this suggested to us that we should consider how such a change would affect the reactivity of the carbido carbon atom. Obviously, an attempt to follow the course of carbonyl migrations accompanied by changes in the Fe_4C cluster geometry is well outside the scope of our calculations, but we can consider several specific model clusters and thus gain considerable insight into the way in which a ketylidene could be formed. First we simply remove the bridging carbony, leaving the Fe_4C cluster intact. The resulting $Fe_4C(CO)_{12}$ cluster is the same one proposed as an intermediate in the formation of $Fe_4C(CO)_{13}$ from $[Fe_4C(CO)_{12}]^{2-}$. As we saw earlier, the low-lying LUMO in this $Fe_4C(CO)_{12}$ cluster is localized across the backbone iron atoms, and as long as the structure of the Fe_4C cluster is unchanged, the removal of the carbonyl ligand has no significant effect on the carbido carbon orbitals. If, however, we fold back the wingtip iron atoms away from the carbido carbon at the same time that we remove the bridging carbonyl ligand, we find that the character of the LUMO in the $Fe_4C(CO)_{12}$ cluster changes. Calculations for a model $Fe_4C(CO)_{12}$ cluster in which the wingtip iron atoms are folded back to their positions in $[Fe_4(CO)_{12}(C{\cdot}CO_2CH_3)]^-$ show that the LUMO is no longer localized exclusively on the backbone iron atoms but now has considerable carbon p_z character. Thus, as the wingtips of the iron butterfly fold back, the carbido carbon p_z orbital becomes more accessible, and migration of a carbonyl group onto the carbido carbon atom becomes a possibility. Thus these calculations suggest that formation of the ketenylidene would require a distortion in the Fe_4C framework. The necessary folding back of the wingtip iron atoms would considerably weaken both the σ and π interactions between the carbido carbon and wingtip iron atoms, but any new bonding interaction between the carbido carbon and the migrating carbonyl would to some degree compensate this loss. Results of further calculations suggest that once formed, the kentenylidene could be expected to react readily with nucleophiles. Calculations were carried out for a model ketenylidene cluster in which the Fe_4C cluster geometry was that of $[Fe_4(CO)_{12}(C{\cdot}CO_2CH_3)]^-$, and the C–C and C–O distances were taken from the structure of the known ketenylidene $[Fe_3(CO)_9(CCO)]^{2-}$.[19] In this model cluster the carbon atom of the carbonyl group attached to the carbido carbon atom is found to carry a significant positive charge. Such a charge should make the ketenylidene susceptible to nucleophilic attack. Although these calculations should be interpreted with caution, they do suggest that in the reaction system we are considering here (eq 2) any ketenylidene formed from the bridged carbonyl species would be trapped by reaction with methanol. The key to the reactivity of the carbido carbon is the folding back of the wingtip iron atoms. Without this change in structure, the carbido carbon orbitals are inaccessible for bonding to other atoms. In the following discussion of the bonding in the ester, we will explore further the consequences of the change in structure of the iron framework.

4. Bonding in $[Fe_4(CO)_{12}(C{\cdot}CO_2CH_3]^-$. Calculations were carried out for both $[Fe_4(CO)_{12}(C{\cdot}CO_2CH_3)]^-$ and a hypothetical parent cluster $[Fe_4(CO)_{12}]^{2+}$ having the same geometry (i.e., having a dihedral angle of 130°). The level diagrams for these clusters are shown in Figure 5. For purposes of comparison, the level diagram for $[Fe_4C(CO)_{12}]^{2-}$ is also included in Figure 5. Note that although $[Fe_4(CO)_{12}(C{\cdot}CO_2CH_3)]^-$ no longer has C_{2v} symmetry (it is reduced to C_s by the presence of the ester group), the orbitals in Figure 5b are shown with labels reflecting the C_{2v} symmetry of the iron butterfly orbitals. The level diagram for $[Fe_4(CO)_{12}]^{2+}$ (Figure 5a) shows that the iron framework orbitals are little changed by the folding back of the wingtip irons. The t_{2g} block of orbitals remains, the higher energy $3a_2$, $4b_2$, and $5a_1$ iron framework bonding orbitals are occupied (in comparison to the clusters shown in Figure 1 the $3a_2$ orbital is stabilized relative to the $5a_1$ and $4b_2$ orbitals), and the unoccupied $4b_1$, $5b_2$, $6a_1$, and $7a_1$ orbitals have the appropriate character to interact with the carbido carbon orbitals. In a simplified picture of the bonding in $[Fe_4(CO)_{12}(C{\cdot}CO_2CH_3)]^-$ we can describe the interaction between the orbitals of the $[Fe_4(CO)_{12}]^{2+}$ iron butterfly and the three highest energy occupied orbitals of $[CCOOCH_3]^{3-}$, since these three high energy orbitals of

(19) Kolis, J. W.; Holt, E. M.; Shriver, D. F. *J. Am. Chem. Soc.* **1983**, *105*, 7307.

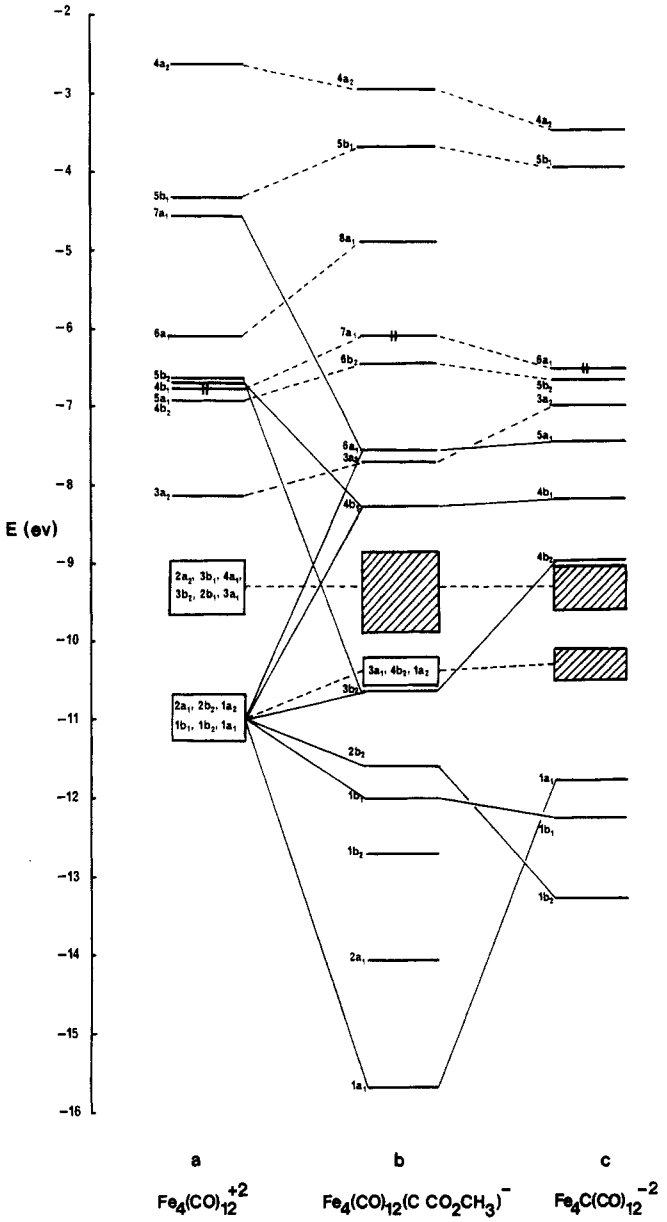

Figure 5. Molecular orbital diagrams for (a) $[Fe_4(CO)_{12}]^{2+}$, (b) $[Fe_4(CO)_{12}(C{\cdot}CO_2CH_3)]^-$, and (c) $[Fe_4C(CO)_{12}]^{2-}$. The geometry of the iron butterfly framework in a is the same as that in b. The energy scale and scaling of orbital energies is the same as described in Figure 2.

the isolated ester trianion can be considered, in decreasing energy, as localized on the terminal carbon in p_x, p_y, and σ lone-pair orbitals. These orbitals thus have the appropriate symmetry to interact with the empty iron cluster orbitals. The actual bonding in the cluster is not quite this simple, however, because only the carbido carbon p_x orbital is uninvolved in bonding within the ester group. The other two carbon p orbitals interact with the adjacent carbon as well as the iron framework orbitals. The carbon p_z orbital is used in σ bond formation to the adjacent carbon, while the planar configuration of the $CCOOCH_3$ group enables the carbon p_y orbital to interact with the adjacent sp^2-hybridized carbon in a π fashion. These changes at the carbido carbon affect the interactions between the carbon and iron framework orbitals. Before discussing these changes in detail, we will first compare the bonding in $[Fe_4(CO)_{12}(C{\cdot}CO_2CH_3)^-$ to that in $[Fe_4C(CO)_{12}]^{2-}$.

In $[Fe_4(CO)_{12}(C{\cdot}CO_2CH_3)]^-$ (Figure 5b), just as in $[Fe_4C(CO)_{12}]^{2-}$ (Figure 5c), the carbon p orbitals interact with iron framework orbitals from both the t_{2g} and e_g sets. These interactions occur in six orbitals ($1a_1$, $1b_1$, $2b_2$, $3b_2$, $4b_1$, and $6a_1$). Once again, there is no net bonding between the carbon p and iron framework t_{2g} orbitals, because the levels containing both the bonding and antibonding interactions between these orbitals are occupied. The net carbon–iron bonding interactions involve the iron framework e_g orbitals. The metal–metal bonding interactions occur in the $3a_2$, $6b_2$, and $7a_1$ orbitals (these orbitals are very similar in character to the $3a_2$, $5b_2$, and $6a_1$ orbitals in $[Fe_4C(CO)_{12}]^{2-}$), and these high-energy occupied orbitals contain no carbon character. Two orbitals $2a_1$ and $1b_2$ occur in Figure 5b that have no counterpart in Figure 5c. These two orbitals are high-lying orbitals associated with the organic group. Since they contain some carbido carbon p_z and p_y character they mix to a small degree with the iron framework a_1 and b_2 orbitals, but they are mainly localized on the carbomethoxymethylidyne portion of the cluster. Both are bonding between the carbido carbon and adjacent carbon atoms. Thus, except for the presence of the these two orbitals, the number and type of orbitals involved in iron–iron and iron–carbon interactions are the same in $[Fe_4(CO)_{12}(C{\cdot}CO_2CH_3)]^-$ as in $[Fe_4C(CO)_{12}]^{2-}$. It can be seen from Figure 5b, however, that the energies and orderings of several of the orbitals involving the carbon–iron interactions are different in $[Fe_4(CO)_{12}(C{\cdot}CO_2CH_3)]^-$. These differences result from both the change in the structure of the Fe_4C cluster and the involvement of the carbido carbon orbitals in bonding to the adjacent carbon. In $[Fe_4(CO)_{12}(C{\cdot}CO_2CH_3)]^-$ the levels involving the interaction between the carbon p_x and metal framework orbitals ($1b_1$ and $4b_1$) appear to be most similar in energy to the corresponding orbitals in $[Fe_4C(CO)_{12}]^{2-}$. This is to be expected, since the carbon p_x orbital is not involved in bonding within the ester group. There is a difference, however, in the nature of the bonding between the carbon p_x and iron framework orbitals in $[Fe_4(CO)_{12}(C{\cdot}CO_2CH_3)]^-$. This can be seen from the Fe–C overlap populations shown in Table I. As a consequence of the folding back of the wingtip irons in $[Fe_4(CO)_{12}(C{\cdot}CO_2CH_3)]^-$ there is no longer any substantial π bonding between the carbon p_x orbital and the wingtip irons. This decreased interaction with the wingtip irons is accompanied, however, by an increased interaction with the backbone iron atoms.

As we noted above, the bonding between the carbido carbon p_z and p_y and iron framework orbitals is affected by both the change in the iron butterfly structure and the presence of the carbomethoxy group. Consider first how these changes affect the bonding of the carbon p_z orbital. Interactions between this orbital and the iron framework orbitals occur in the $1a_1$ and $\mathbf{6a_1}$ molecular orbitals. A comparison of parts b and c of Figure 5 shows that the $1a_1$ orbital in $[Fe_4(CO)_{12}(C{\cdot}CO_2CH_3)]^-$ is considerably stabilized relative to the corresponding orbital in $[Fe_4C(CO)_{12}]^{2-}$ and lies lower in energy than the two ester based orbitals $2a_1$ and $1b_2$. The $1a_1$ orbital now contains carbon s as well as p_z character, suggesting sp hybridization of the carbon. It should also be noted that the $1a_1$ orbital is delocalized over the ester group so that although this orbital is bonding between the carbon and iron butterfly, the iron character is significantly smaller than it is in the corresponding $1a_1$ orbital in $[Fe_4C(CO)_{12}]^{2-}$. The carbido carbon p_z orbital also contributes to the $2a_1$ orbital (see Figure 5b). As noted above, this orbital is localized on the organic group and is bonding between the carbido carbon and adjacent carbon atoms. It has little metal character. Thus the carbon p_z orbital, stabilized by its participation in bonding within the carbomethoxy group, interacts less effectively with the iron framework orbitals than it does in the μ_4-carbido

clusters. This decreased interaction is reflected in the Fe–C p_z overlap populations listed in Table I. In $[Fe_4(CO)_{12}(C{\cdot}CO_2CH_3)]^-$ the interactions between the carbon p_z orbital and the backbone irons has diminished and the π interaction between the carbon p_z orbital and the wingtip irons has disappeared.

In $[Fe_4(CO)_{12}(C{\cdot}CO_2CH_3)]^-$, the interactions between the carbon p_y and iron framework orbitals occur in the $2b_2$ and $3b_2$ orbitals (counterparts of the $1b_2$ and $4b_2$ orbitals of $[Fe_4C(CO)_{12}]^{2-}$). Since the carbido carbon no longer lies directly between the wingtip iron atoms, these interactions, particularly those involving the metal t_{2g} orbitals, are weaker in $[Fe_4(CO)_{12}(C{\cdot}CO_2CH_3)]^-$ than in $[Fe_4C(CO)_{12}]^{2-}$. One consequence of this is the reduced separation in energy between the $2b_2$ and $3b_2$ orbitals (the bonding and antibonding partners with respect to the interaction between the carbon p_y and cluster t_{2g} orbitals). This shift in the energy levels has little effect on the overall bonding between the carbon and metal framework, because the net bonding interaction between the carbon p_y and iron t_{2g} orbitals is negligible. It is important to observe, however, that the interaction between the carbon p_y and iron framework e_g orbitals is also weaker in $[Fe_4(CO)_{12}(C{\cdot}CO_2CH_3)]^-$. This weakened interaction is reflected in the C (p_y)–Fe overlap populations, (Table I). The folding back of the wingtip iron atoms results in the total overlap population between the C p_y and wingtip iron orbitals being about 25% smaller in $[Fe_4(CO)_{12}(C{\cdot}CO_2CH_3)]^-$ than in $[Fe_4C(CO)_{12}]^{2-}$. It is also important to note that while the bonding interaction between the carbido carbon p_y and wingtip iron orbitals is somewhat weaker in $[Fe_4(CO)_{12}(C{\cdot}CO_2CH_3)]^-$, the planar configuration of the ester group and the sp^2 hybridization of the carbon atom attached to the carbido carbon atom allow the development of some double-bond character between the two carbon atoms. The $1b_2$ level seen in Figure 4b is in fact π bonding between these two carbon atoms. The carbon p_y oribital is thus stabilized by its interaction with both the metal framework and the adjacent carbon.

The major result of all these changes in the interactions between the carbon p and iron framework orbitals is the weakened bond between the carbon and wingtip iron atoms in $[Fe_4(CO)_{12}(C{\cdot}CO_2CH_3)]^-$. This is reflected in the total overlap populations shown in Table I. In $[Fe_4C(CO)_{12}]^{2-}$ the total C(p)–Fe overlap populations are about 50% larger for the wingtip irons than for the backbone irons. Now in $[Fe_4(CO)_{12}(C{\cdot}CO_2CH_3)]^-$ the total C(p)–Fe overlap population for the wingtip irons is only half as large as in the dianion and is actually smaller than the value for the backbone irons. We should also note, however, that while the interaction between the wingtip irons and the carbido carbon is weaker in $[Fe_4(CO)_{12}(C{\cdot}CO_2CH_3)]^-$ than in the μ_4-carbido clusters, the interaction between the wingtip and backbone irons is stronger. This is reflected in shorter Fe–Fe bond lengths, stabilization of the $3a_2$ metal–metal bonding orbital, and increased overlap populatioins between the wingtip and backbone irons in $[Fe_4(CO)_{12}(C{\cdot}CO_2CH_3)]^-$.

In summary, the bonding in $[Fe_4(CO)_{12}(C{\cdot}CO_2CH_3)]^-$ reflects both the presence of the carbomethoxy group and the distortion of the iron butterfly. These two factors are of course not really independent since we would expect the geometry within the cluster to optimize both the interactions within the iron butterfly and the interaction of the carbon orbitals with the ester group and the iron butterfly. The carbon p_x orbital, which takes no part in the ester bonding, interacts most strongly with the cluster orbitals. At the other extreme, the carbon p_z orbital, which is involved in σ bond formation to the adjacent carbon, is less available for bonding to the iron cluster and contributes least of the three carbon p orbitals to bonding with the iron framework orbitals. In comparison to the μ_4-carbido clusters, the π interactions between the carbon p_x and p_z orbitals and the wingtip irons are lost, so that in $[Fe_4(CO)_{12}(C{\cdot}CO_2CH_3)]$ the carbon p_x and p_z orbitals interact with only the backbone iron atoms. The σ interaction between the carbon p_y orbital and the wingtip iron atoms is also weaker in $[Fe_4(CO)_{12}(C{\cdot}CO_2CH_3)]^-$ than in the μ_4-carbide and is now comparable to the interaction between the carbon p_x, and backbone iron orbitals. This weakened σ interaction is accompanied by the development of a π interaction with the adjacent sp^2-hybridized carbon in the carbomethoxy group. A measure of the importance of this π interaction may be found in the fact that all of the C-derivitized Fe_4C clusters involve an sp^2-hybridized carbon bound to the methylidyne carbon. It is particularly interesting to note that the reaction which might have led to an sp^3-hybridized carbon bonded directly to the carbido carbon was reported by Shriver[12] to yield only the tetrahedral μ_3-ethylidyne derivative (eq 3). We will address this aspect of the bonding and reactivity of Fe_4C clusters in a subsequent paper.

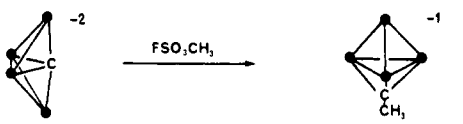

$[Fe_4C(CO)_{12}]^{2-}$ $[Fe_4(CO)_{12}(CCH_3)]^-$ (3)

Conclusions

The structure of the μ_4-carbido Fe_4C clusters allows strong interactions between the carbido carbon p orbitals and both the wingtip and backbone iron atoms. These interactions stabilize the molecular orbitals containing significant carbido carbon character so that the frontier orbitals are metal in character. Thus most of the reactivity of $[Fe_4C(CO)_{12}]^{2-}$ centers around the metal framework and not the carbido carbon atom. Reactions of $Fe_4C(CO)_{13}$ which do result in derivitization of the carboido carbon atom require a change in geometry of the iron butterfly, namely an opening of the butterfly. This change in geometry, which results in a weakening of the interactions between the carbido carbon p orbitals and the wingtip iron atoms, makes the carbon p orbitals more accessible for bonding to a substituent.

During the preparation of this paper we became aware of another theoretical study of metal cluster carbides, using a somewhat different approach, by Hoffmann and coworkers.[20] They report a general study of the reactivity of butterfly and square-pyramidal transition-metal cluster carbides, while we have focused on several specific butterfly clusters and their chemistry. For those examples which our two studies have in common, many of our conclusions are similar.

Acknowledgment. We are grateful to Prof. Michael B. Hall for making available to us a copy of his computer program utilizing the Fenske–Hall technique and to Prof. Roald Hoffmann for sending us a copy of his paper prior to publication.

Registry No. $[Fe_4C(CO)_{12}]^{2N}$, 74792-04-4; $[Fe_4(CO)_{12}(C{\cdot}CO_2CH_3)]^-$, 89936-19-6; $[HFe_4C(CO)_{12}]^-$, 74792-02-2; $Fe_4C(CO)_{13}$, 79061-73-7; Fe, 7439-89-6.

(20) Wijeyesekera, S. D.; Hoffmann, R.; Wilker, C. N., submitted for publication in *Organometallics*.